A highly ordered, aromatic bidentate self-assembled monolayer on Au(111): a combined experimental and theoretical study

Xia Stammer,[a] Katrin Tonigold,[b] Asif Bashir,[c] Daniel Käfer,[d] Osama Shekhah,[a] Christian Hülsbusch,[d] Martin Kind,[e] Axel Groß*[b] and Christof Wöll*[a]

Received 1st February 2010, Accepted 26th April 2010
First published as an Advance Article on the web 14th May 2010
DOI: 10.1039/c002215m

Self assembled monolayers (SAMs) made from an aromatic organodithiol, 2-mercaptomethylbenzenethiol ($C_6H_4SHCH_2SH$) on Au(111) have been investigated in the context of a combined experimental and theoretical approach. The SAMs prepared by immersion of an Au-substrate in corresponding ethanolic solutions were characterized using scanning tunneling microscopy (STM), X-ray photoelectron spectroscopy (XPS), infrared reflection absorption spectroscopy (IRRAS) and thermal desorption spectroscopy (TDS). Adapted from the experimentally obtained unit cell of the SAM, density functional theory (DFT) calculations were applied to get a deeper insight into the structure of these dithiolate based SAMs. On the basis of the experimental and theoretical findings we provide a detailed structural model for this aromatic SAM consisting of the phenyl-group rigidly anchored to the substrate by two thiolate-bonds.

Introduction

Self-assembled monolayers (SAMs), especially those made from thiols chemisorbed on gold, have been attracting huge interest for more than 25 years, because of their ease of preparation and potential applications in many fields like electrochemistry, lubrication, friction *etc*.[1–3] Initially most of the SAMs investigated in the beginning were made from organothiols of rather easy composition, like alkane-1-thiols.[4–6] In recent years, the focus of interest has moved to functionalized SAMs that open many possibilities for surface anchoring.[7–9] Not only the termination of the organothiol but also the anchor group influences the properties of the SAM. Besides the frequently used monothiols, SAMs on gold can also be prepared from dithiols,[10–12] disulfides[13] or cyclic disulfides.[14–17] The earliest publications on SAMs report the adsorption of cyclic disulfides on Au forming two Au–S bonds per molecule.[14]

Such dithiols can be used to achieve different aims: while α,ω-organodithiols can be used to prepare SH-terminated organic surfaces, *e.g*. to deposit metal atoms,[18,19] organothiols with two thiol-groups relatively close to each other can form organic monolayers with both sulfur atoms forming bonds to the substrate surface leading to a more rigid, bidentate-type anchoring to the substrate. Such SAMs have been studied in the past, *e.g*., to vary the density of organic moieties extending from the surface and thus the van der Waals interaction between neighboring chemisorbed molecules.[11,20–26] In many cases SAMs fabricated from this kind of dithiols are less well ordered than their monothiol counterparts, a fact that is frequently attributed to the increased binding energy and a correspondingly increased activation energy for lateral diffusion.[11,20,21,23,27,28] Specifically designed dithiols have been used to prepare mixed SAM surfaces with a precise control of the composition, which is normally not possible, because of the different adsorption properties of unequal monoorganothiols on the substrate surface.[21,28] In some studies, SAMs have been prepared from dithiols with a rigid molecular structure, which forces the two sulfur atoms to a fixed distance that differs from the spacing of hollow site positions on the Au(111) surface, in order to study the influence of different adsorption sites on gold.[16,29–32]

Small aromatic dithiols, such as phenyl-dithiols with two SH- or CH_2SH-groups on *meta*- or *para*-positions, adsorbed on colloidal gold have been investigated using surface enhanced Raman spectroscopy (SERS) and electrochemical methods. The structure of the adsorbed films was found to depend strongly on the concentration of the molecules in aqueous solutions.[33–37]

SAMs produced from organodithiols on gold typically show a poor lateral order only. To our knowledge, no studies have been published where molecular resolution in STM could be obtained for SAMs based on a bidentate phenyl-dithiol on an Au(111) surface. In this work, we present a joint experimental and theoretical investigation of 2-mercaptomethylbenzenethiol (MMBT) on Au(111). The structure of the molecule and a proposed simplified structure of the SAM formed by MMBT on Au(111) are shown in Fig. 1.

[a] *Institute of Functional Interfaces, Karlsruhe Institute of Technology, 74800 Karlsruhe, Germany*
[b] *Institut für Theoretische Chemie, Universität Ulm, 89081 Ulm, Germany*
[c] *Interface Chemistry and Surface Engineering, Max-Planck-Institut für Eisenforschung, 40237 Düsseldorf, Germany*
[d] *Lehrstuhl Physikalische Chemie I, Ruhr-Universität Bochum, 44780 Bochum, Germany*
[e] *Institut für Anorganische und Analytische Chemie, Goethe-Universität Frankfurt, 60438 Frankfurt am Main, Germany*

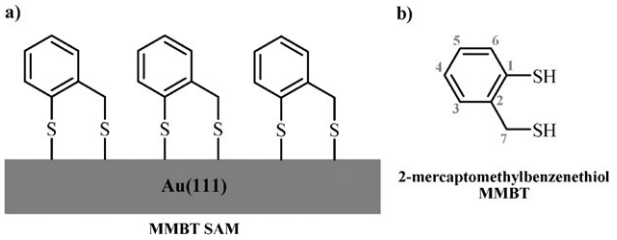

Fig. 1 Schematic drawing of (a) the investigated MMBT SAM and (b) the compound MMBT used to prepare the SAM.

Experimental

Synthesis of 2-mercaptomethylbenzenethiol (MMBT)

The mercaptomethyl functionalized benzenethiol **3** (see Fig. 2) can be easily received in reasonable yields, as similarly described by E. Klingsberg *et al.* and A. G. Hortmann *et al.*[38,39] Treatment of 2,2′-dithiosalicylic acid **1** with phosphorus(v) sulfide in pyridine gives 3*H*-1,2-benzodithiole-3-thione **2**. Reduction of **2** with lithium aluminium hydride in diethyl ether gives 2-mercaptomethylbenzenethiol **3**.

The following spectrometers were used for the NMR characterisation: ^{1}H NMR/^{13}C NMR spectra-Bruker DPX 200/Bruker DRX 400; FAB-/EI-mass spectra-VG AutoSpec. All solvents were purified and dried according to a standard procedure. All reactions were carried out under an atmosphere of argon. Chromatography was performed on ICN silica 32–63 μm, 60 Å. Commercially available chemicals were obtained from Acros and Aldrich.

3*H*-1,2-Benzodithiole-3-thione (2). To a solution of 2,2′-dithiosalicylic acid **1** (20 g, 65.3 mmol) in pyridine (150 mL) phosporus(v) sulfide (20 g, 45 mmol) was added. The solution was refluxed for 1 h. After cooling to room temperature the suspension was filtered and washed with cold ethanol (*ca.* 5 °C). The resulting product was dried in vacuum. Yield: 13.26 g (55%, orange crystals). ^{1}H NMR (400.13 MHz, [D_6]DMSO, 30 °C): δ = 8.13 (m, 1H, aromatic), 8.06 (m, 1H, aromatic), 7.83 (m, 1H, aromatic), 7.55 (m, 1H, aromatic) ppm. ^{13}C NMR (100.62 MHz, [D_6]DMSO, 30 °C): δ = 216.79, 152.94, 140.39, 133.18, 127.24, 126.35, 125.15 ppm. MS (FAB): m/z = 184.9 [**2** + H]$^{+}$.

2-Mercaptomethylbenzenethiol (3). To a suspension of lithium aluminium hydride (2 g, 53 mmol) in diethyl ether (50 mL) a solution of 3*H*-1,2-benzodithiole-3-thione **2** (4.6 g, 25 mmol) in a mixture of diethyl ether and tetrahydrofuran (150 mL, 1/1) was added dropwise within 1 h. The reaction mixture was stirred for 18 h at room temperature. After cooling to 0 °C, the excess of lithium aluminium hydride was decomposed with 2-propanol. The mixture was acidified with sulfuric acid (10% w/w, 50 mL) and extracted with diethyl ether. The organic phase was washed with brine (2 × 50 mL), dried over anhydrous sodium sulfate and filtered. The solvent was removed in vacuum and the resulting oily liquid product was separated by column chromatography on silica (2.5 × 50 cm^2, dichloromethane). Yield: 2.43 g (62%, yellow liquid). ^{1}H NMR (200.13 MHz, $CDCl_3$, 30 °C): δ = 7.20–7.48 (m, 4H, Ar–H), 3.94 (d, 2H, C*H*$_2$–SH), 3.79 (s, 1H, Ar–SH), 1.99 (t, 1H, CH$_2$–S*H*) ppm. ^{13}C NMR (50.33 MHz, $CDCl_3$, 30 °C): δ = 139.61, 131.95, 129.99, 129.34, 127.89, 126.79, 28.24 ppm. MS (EI): m/z = 155.9 [**3**]$^{+}$.

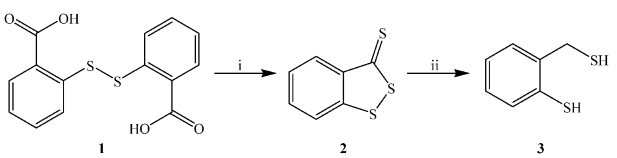

Fig. 2 Synthesis of 2-mercaptomethylbenzenethiol **3**: (i) P_4S_{10}, pyridine, reflux, 1 h; (ii) $LiAlH_4$, Et_2O, THF, RT, 18 h.

Preparation of self-assembled monolayers

The self-assembled monolayers were prepared by immersing Au(111) substrates in 1 mM (for STM) and 50 μM (for other methods) ethanolic solutions of MMBT for 15–24 h. Stock solutions with a concentration of 1 mM were produced by dissolving MMBT in degassed absolute ethanol and stored under Ar at around 5 °C. The deposition solutions for IRRAS, XPS and TDS were obtained by diluting the stock solutions with degassed ethanol to a concentration of 50 μM.

The substrates for the IRRAS and XPS experiments were prepared by depositing 50 Å titanium (Chempur, 99.8%) and 1500 Å gold (Chempur, 99.995%) layers onto clean Si(100) wafers (Wacker) in vacuum using a Leybold Univex 300 metal evaporator. For STM and TDS measurements, freshly cleaved mica sheets (Mahlwerk Neubauer-Friedrich Geffers) were heated for about 48 h and subsequently coated with 1400 Å of gold by thermal evaporation at 280 °C in vacuum. The Au(111) substrates were stored in a desiccator before application. Immediately before the SAM preparation for STM measurements, the gold on mica substrates were flame annealed using a butane/O_2 burner in order to yield well-defined terraces. After immersion of the substrates into the MMBT solutions, the resulting SAMs were exhaustively rinsed with ethanol and dried under a flow of gaseous nitrogen before characterization. For STM investigation, some samples were annealed to 70 °C in vacuum either for 1 h or overnight (about 15 h) before measurements.

IR measurements

ATR bulk spectra of MMBT were recorded using a Jasco FT/IR-4100 spectrometer equipped with a ZnSe ATR unit and a DTGS detector. The resolution was 2 cm^{-1}. IRRAS data for the SAMs were recorded at atmospheric pressure with a Biorad Excalibur FTS-3000 FTIR-spectrometer equipped with a liquid-nitrogen cooled narrow band MCT detector and a purge gas generator. All IRRAS data were recorded with a resolution of 2 cm^{-1} using p-polarized radiation at an incidence angle of 80° relative to the surface normal. SAMs of perdeuterated 1-hexadecanethiol on Au have been used as reference in the IRRAS experiments. In some additional experiments, a UHV apparatus combined with a Bruker VERTEX 80v FTIR-spectrometer, which is equipped with a heatable holder, was used. The UHV IRRAS experimental setup has been described elsewhere.[8,40–42]

XPS measurements

A UHV apparatus based on a modified Leybold XPS system with a double-anode X-ray source was used to obtain X-ray photoelectron spectra at room temperature. For the measurements reported here the Al Kα X-ray source ($h\nu$ = 1486.7 eV) was used at an incident angle of 45° relative to the surface normal and the detector was positioned perpendicular to the sample surface.[43] The binding energies were calibrated by setting the Au $4f_{7/2}$ binding energy to 84.0 eV and the peak intensities were quantified by standard curve-fitting software using Shirley background subtraction and Gaussian-Lorentzian profiles. The fits of the Au lines were performed with fixed energy splitting and ratios of peak areas. To estimate the thickness of the monolayers, a decane-1-thiol SAM on a similar gold substrate with a well-known thickness of 13.1 Å has been used as a reference.[44]

STM measurements

STM data were acquired using a Jeol JSPM 4210 microscope. The tips were prepared by cutting a 0.25 mm Pt/Ir (80 : 20, Chempur) wire mechanically. All STM micrographs were recorded in air at room temperature in constant current mode. With respect to the sample the tunneling current varied from 60 to 200 pA and the sample bias from 500 to 900 mV. No tip-induced changes were observed for these tunneling conditions.[45] All STM data correspond to unfiltered, uncorrected raw data. As a result, thermal drifts are not compensated for and can lead to a distortion of the rectangular unit cells of the SAM superlattices.

TDS measurements

The TDS measurements were carried out in a multi-technique UHV instrument with an analytical chamber based on a Leybold MAX100 system described elsewhere.[46] A quadrupole mass spectrometer (Balzers QMS200, mass range 0–300 amu) with a Feulner cup was used to record TD spectra.[47] The sample holder was heated by electron bombardment and the temperature has been varied between 300 and 750 K by employing a computer controlled linear heating ramp of β = 0.5 K s^{-1}. For the temperature measurement a chromel/alumel (K-type) thermocouple was used. TDS spectra were recorded for m/z = 32, 64, 90, 122 and 154 amu. To improve the signal-to-noise ratio seven spectra for each m/z value were recorded and then averaged.

Computational details

Periodic DFT calculations have been performed using the Vienna *ab initio* simulation package (VASP).[48,49] Electron–electron exchange and correlation interactions have been described within the generalized gradient approximation (GGA) by employing the functional of Perdew, Burke and Ernzerhof (PBE).[50] In order to account for electron–ion interactions the projector augmented wave (PAW) method has been used.[51,52] The electronic one-particle wave functions were expanded in a plane wave basis set up to an energy cut-off of 400 eV. The metal surface was modeled by a slab consisting of five atomic layers that were separated by a vacuum region of 25 Å. The interlayer spacing in the surface was taken from the theoretical lattice parameter calculated for bulk gold (4.171 Å).

According to experimental results, the adsorption of MMBT has been modeled by a $(3 \times \sqrt{3})$ rectangular unit cell of the overlayer structure. A (4 × 9 × 1) Monkhorst–Pack k-point mesh with a Methfessel-Paxton smearing of 0.1 eV was applied for the integration over the first Brillouin zone. The k-point meshes of other unit cells used for comparison have been adjusted correspondingly. The geometry of the adsorption complex was optimized by relaxing all atoms of the adsorbate and the metal atoms of the two uppermost layers of the surface. Calculations of isolated molecules employed a large cell (20 Å × 21 Å × 22 Å), an integration using the Γ-point only and a Gaussian smearing of 0.1 eV.

Energetics

The interaction energy between MMBT and the substrate can be described with respect to different reference states. The energy needed to break the covalent bond between gold and sulfur is defined as binding energy

$$E_{\mathrm{bind}} = E_{\mathrm{Au(111)}} + E_{\mathrm{MMBT\text{-}radical}} - E_{\mathrm{Au(111)\text{-}MMBT}} \quad (1)$$

where $E_{\mathrm{Au(111)}}$ is the energy of the clean surface, $E_{\mathrm{MMBT\text{-}radical}}$ is the energy of the isolated MMBT diradical and $E_{\mathrm{Au(111)\text{-}MMBT}}$ denotes the total energy of the relaxed adsorption complex.

As the desorption process might take place *via* the formation of a dithiolane system, the desorption energy is defined as

$$E_{\mathrm{des}} = E_{\mathrm{Au(111)}} + E_{\mathrm{dithiolane}} - E_{\mathrm{Au(111)\text{-}MMBT}}. \quad (2)$$

Here $E_{\mathrm{dithiolane}}$ represents the energy of the isolated dithiolane system.

To further improve comparison to experimental desorption energies, corrections for dispersive effects that are missing in current density functionals have to be included.[53] We applied the DFT-D approach by adding an empirical dispersion correction *ex post* to the energy of optimized structures. The empirical dispersion correction is calculated as

$$E_{\mathrm{dispersion}} = -s_6 \sum_i \sum_j \frac{C_6^{ij}}{R_{ij}^6} f_{\mathrm{damp}}(R_{ij}). \quad (3)$$

The scaling factor s_6 and the C_6^{ii} coefficients of non-metallic atoms needed to calculate the dispersion coefficient of mixed atom pairs *via*

$$C_6^{ij} = \sqrt{C_6^{ii} C_6^{jj}} \quad (4)$$

were taken from Grimme.[54]

For dispersive interactions between molecules also the form of the damping function f_{damp} was taken from ref. 54.

As far as dispersive interactions between the molecules and the Au surface are concerned, the ansatz for the damping function was slightly modified in order to account for screening effects of the metal. The distance between the individual metal atoms and the atoms of the molecules (R_{ij}) is replaced

by the distance between the atoms of the molecule and the (uppermost) surface (layer) of Au. The procedure used to determine the C_6^{ii} coefficient for Au will be described elsewhere.

Simulation of IR spectra

Vibrational frequencies and normal modes were obtained by using the harmonic approximation within the finite-difference method. All atoms of the molecule were subsequently displaced along all three spatial coordinates by ±0.02 Å. The resulting restoring forces on the atoms were used to set up the Hessian matrix. For each normal mode of vibration the IR intensity was calculated as the square of the derivative of the dipole moment. In case of the isolated molecule the dipole moment along all three spatial coordinates was considered. As far as the adsorbed molecule is concerned, only the dipole moment component along the surface normal was taken into account, since the dipole moment components parallel to the surface are extinguished by screening effects and thus cannot contribute to the probability of the spectroscopic transition (surface selection rule). For comparison the IR spectra of the isolated molecule was also calculated using analytical second derivatives as implemented in the GAUSSIAN program package.[55] No significant changes between the IR spectra of the isolated MMBT simulated with the two different methods were found.

Simulation of STM images

STM simulations are based on the Tersoff-Hamann approximation.[56] Within that model the tunneling current is proportional to the local density of states (LDOS) at the surface close to the Fermi energy at the position of the tip. Constant-current images are simulated by an isosurface of the LDOS integrated between the Fermi energy of the system and the sample bias.

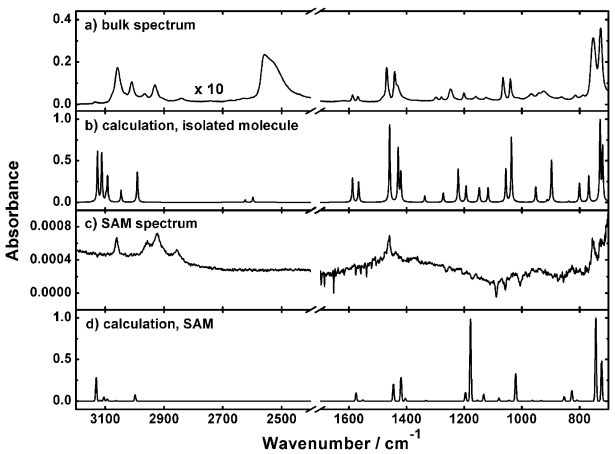

Fig. 3 Experimental and calculated IR spectra of MMBT species. (a): bulk IR spectrum of MMBT recorded with an ATR unit. (b): calculated spectrum of an isolated MMBT molecule. (c): atmospheric pressure IRRA spectrum of the MMBT SAM on Au(111). (d): calculated spectrum of the MMBT SAM on Au(111). See text for discussion.

Results and discussion

IR spectra of MMBT and MMBT-SAMs

Fig. 3 shows the experimental and calculated IR spectra of bulk MMBT and the MMBT-SAM on Au(111).

Vibrational frequencies and relative intensities of the absorption bands in the experimental bulk spectrum (panel a) and the calculated spectrum of an isolated MMBT molecule (panel b) are in good agreement. The positions of the CH and SH stretching modes above 2500 cm^{-1} in the calculated spectrum differ markedly from the experimental data, but the agreement is still good enough so that all bands could be assigned based on the calculation results (see Table 1). No scaling factor was used to adjust the experimental and calculated IR spectra obtained in the harmonic approximation using finite differences. On the other hand, PBE is known to overestimate covalent binding energies. Hence it is not surprising that the wave numbers of the CH and SH stretching modes above 2500 cm^{-1} are much larger in the calculated spectrum compared to the experimental data.

In the experimental IRRAS data for the MMBT-SAM (panel c in Fig. 3) no additional bands compared to the bulk spectrum can be found. The intense absorption bands of MMBT are still visible in the SAM spectrum, except the SH stretching modes **6** and **7**, which is in accordance with the assumption that upon adsorption of the dithiol the SH bonds are cleaved and both sulfur atoms form new bonds with the gold substrate. Some other major bands in the SAM spectrum (**11**, **15**) are either invisible or clearly attenuated in the spectrum of the SAM. This phenomenon can be explained by the surface selection rule, which states that IR bands with a transition dipole moment (TDM) oriented parallel to a metal surface are strongly attenuated in intensity.[57,58] From the attenuation of vibrational bands in the SAM spectrum, conclusions can be drawn on the orientation of the adsorbed molecule relative to the substrate surface. For such analysis, the directions of the TDMs relative to the molecular frame must be known. The TDM directions can be determined either from symmetry consideration or by analyzing theoretical results. However, the analysis of the theoretical results is hampered by the fact that the TDM directions of many modes depend on the CSH twist angles which strongly vary even for very small geometry changes. Since the conformation of adsorbed MMBT is very likely to be different from the one of the isolated MMBT and because upon adsorption the molecule loses the thiol H atoms, the usefulness of the TDM directions obtained from the theoretical results is somewhat restricted.

Nevertheless, some hints on the orientation of the adsorbed molecule can be obtained from the experimental SAM spectrum using the results of the vibrational calculations for the isolated molecule and some general simplifying assumptions about vibrational modes of isolated moieties like the aromatic ring and the methylene group: at first, two intense bands below 800 cm^{-1} (**16** and **17**) are not attenuated in the SAM spectrum. These signals are due to intense out-of-plane bending modes of the aromatic ring with only minor influence of vibration of the CH_2 moiety. According to DFT

Table 1 Band assignments of MMBT IR spectra. Letters in parentheses refer to the signal strength (vs = very strong, s = strong, m = medium, w = weak, and vw = very weak). The band assigned with * is a shoulder. The shortcuts ip and op denote "in plane" and "out of plane", respectively

	Wavenumber/cm^{-1}				
No	Bulk (experimental)	Isolated molecule (calculation)	SAM (experimental)	SAM (calculation)	Assignment
1	3059 (w)	3127 (vs)	3062 (s)	3131 (w)	Aromatic CH stretch
2	3010 (w)	3112 (s)		3117 (vw)	Aromatic CH stretch
3	2965 (w)	3096 (m)	2957 (m)	3100 (w)	Aromatic CH stretch
4	2931 (w)	3046 (m)	2923 (s)	3065 (vw)	CH_2 asym stretch
5	2843 (w)	2991 (w)	2857 (m)	2998 (w)	CH_2 sym stretch
6	2558 (w)	2624 (w)			SH stretch
7	2525 (w)*	2598 (w)			SH stretch
8	1587 (w)	1588 (m)		1575 (w)	Ring ip bend
9	1569 (w)	1566 (m)		1552 (vw)	Ring ip bend
10	1469 (s)	1459 (vs)	1459 (s)	1446 (m)	Ring ip bend
11	1441 (s)	1429 (s)	1438 (w)	1419 (m)	Ring ip bend
12	1248 (m)	1221 (s)		1196 (w)	CH_2 wagging + ring ip bend
13	1201 (w)	1194 (w)		1178 (s)	CH_2 wagging + ring ip bend
14	1066 (s)	1056 (m)		1045 (vw)	Ring ip bend + CH, SH bend
15	1040 (s)	1036 (s)		1022 (m)	Ring ip bend
16	753 (vs)	729 (vs)	755 (vs)	744 (vs)	CH_2 wagging + ring op bend
17	727 (vs)	742 (m)	723 (vs)	724 (s)	CH_2 rock + ring op bend

calculations, the TDMs of these modes do not markedly change their directions for different conformations of the isolated molecule. Both TDMs are parallel to the normal of the aromatic ring. From the fact that the modes **16** and **17** are not attenuated in the SAM spectrum the conclusion can be drawn that the aromatic ring cannot be totally upright but must to some extent be tilted with respect to the surface. Two bands near 1450 cm^{-1} (**10** and **11**) have almost the same intensities in the bulk spectrum, while band **11** is markedly attenuated in the SAM spectrum. Both signals are due to in-plane bending modes of the aromatic ring whose TDMs both are parallel to the ring plane but not parallel to each other. For modes **16** and **17**, the directions of the TDMs are almost constant in the results of vibrational calculations of different conformations of the isolated MMBT molecule. The attenuation of only one of those bands is in accordance with the assumption that the adsorbed molecules have a uniform orientation relative to the substrate surface (with the TDM of the attenuated band oriented more parallel, the TDM of the other band oriented more upright with respect to the surface). In the region around 3000 cm^{-1}, the aromatic CH stretching mode **2** is attenuated in the experimental spectrum of the SAM. According to calculation results, the TDM of this mode is almost perpendicular to the TDM of mode **1** which is not attenuated. This result further corroborates the assumption of a uniform orientation of the adsorbed molecules.

Two strong bands in the bulk spectrum at about 1050 cm^{-1} (**14** and **15**) are completely absent in the SAM IR-data. In this region, only some negative bands related to the reference SAM (a perdeuterated hexadecane-thiolate SAM on gold) are located. Although this might spoil the detection of vibrational modes of the sample, we believe that the bands **14** and **15** in the SAM spectrum are at least partially attenuated. This cannot be easily explained within the simplified picture of TDMs of the adsorbed molecule being identical to the ones of the isolated molecule.

Additionally an IR spectrum of the MMBT SAM was simulated (see panel d of Fig. 3). Compared to the simulated IR spectrum of the isolated MMBT molecule many vibrational bands are damped due to a diminishing TDM component perpendicular to the surface. Other bands like the in-plane (**11**) or out-of-plane (**16** and **17**) bending modes of the aromatic ring are not attenuated. Nevertheless, there are obvious discrepancies compared to the experimental spectrum. In the simulated SAM spectrum band **11** is not attenuated in comparison with band **10**. The most striking difference is that the simulation predicted the CH_2 wagging mode (**13**) to be the most intense absorption band, which cannot be found in the measured IRRA spectrum. A further discrepancy is the absence of band **15** in the experimental SAM spectrum. The reason for these discrepancies remains unclear at present. It should be noted, however, that to our knowledge there are only few examples where theoretical IR-spectra have been computed for a thiolate SAM adsorbed on an Au substrate.[59,60] They also reveal discrepancies between calculated and experimental IR frequencies and intensities. In fact, there may be systematic problems related to this procedure. Preliminary results obtained from MD simulations indicate that the discrepancies are reduced if the IR spectra are calculated directly as Fourier transform of the dipole autocorrelation function obtained from *ab initio* molecular dynamics trajectories obtained at room temperature. This indicates that the thermal motion of the molecules has a significant influence on the vibrational spectra.

In order to check the thermal stability of the SAMs and to achieve comparable preparation conditions to the annealed SAMs on mica for the STM measurements, UHV IRRA spectra were recorded at room temperature and after annealing the same sample to 70 °C for about 2 h (data not shown here). Since no change was found in the spectra, especially not in the MMBT-SAM characteristic CH stretch regime around 3000 cm^{-1}, we conclude that the monolayer is stable at this elevated preparation temperature.

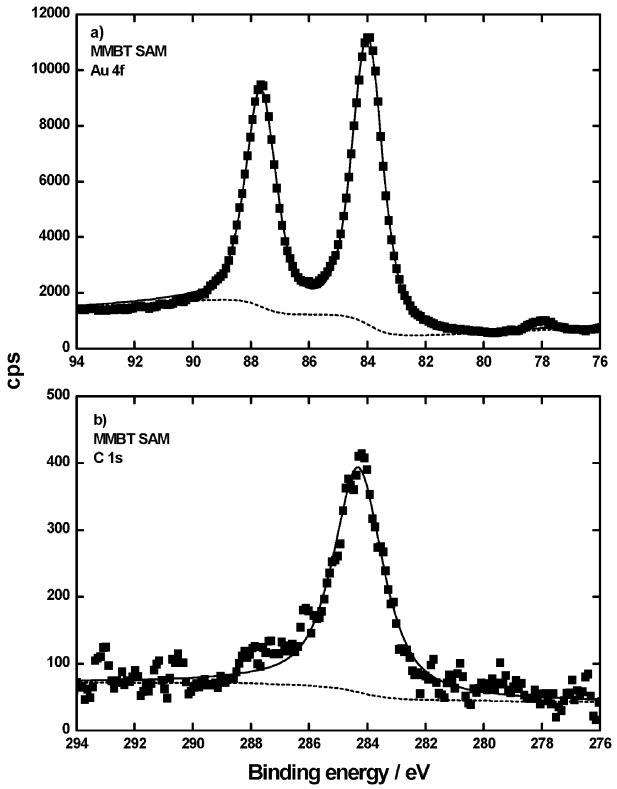

Fig. 4 XPS spectra of a MMBT SAM on Au(111). (a) and (b): Au 4f and C 1s lines of the MMBT SAM. All lines were fitted to Gaussian-Lorentzian profiles after subtraction of a Shirley background. The fits of the Au lines were performed with fixed energy splitting and ratio of peak areas.

XPS data of MMBT-SAMs

XPS data were acquired for the MMBT-SAM and a decane-1-thiolate SAM. The Au 4f lines of the underlying gold substrates have been measured for each sample with the binding energy of the Au $4f_{7/2}$ line set to 84.0 eV. In the C 1s spectrum for a decane-1-thiol SAM a single peak at 284.3 eV is observed and the one of the MMBT-SAM shows a similar peak at the same position, because the binding energies of the methylene carbon and the carbon atoms of the phenyl ring are too close to each other to be resolved with the present experimental resolution of 1 eV. The carbon and the gold regions of the MMBT-SAM are displayed in Fig. 4. In previous work it has been demonstrated that the thickness of organothiolate SAMs can be determined from the relative intensities of the Au and the C XPS peaks by using a reference system.[18,45,61] In the present case the Au4f/C1s ratio amounts to 29.1, significantly larger than that determined on the same apparatus for a decanethiolate-based SAM (22.0) and a pyridine-phenyl-based SAM (20.9). In the case of MMBT, however, this analysis cannot be applied in a straightforward fashion since the monomer used to fabricate the SAM contains two S-atoms and the C : S atomic ratio is so small (3.5) that SAMs based on monothiols cannot be used as a reference. We conclude that the high Au4f/C1s XPS intensity ratio is consistent with a MMBT-SAM with a $(3 \times \sqrt{3})$ rectangular unit cell and a thickness of 6.1 Å as obtained from the DFT calculations.

STM images

STM images were collected for MMBT SAMs prepared at room temperature (*ca.* 300 K). As shown in Fig. 5(a) and (b) no etch pits can be observed and no high resolution STM images can be achieved. Even the quality of the STM topography is rather poor. We suppose, because of the bulky anchor group the pre-adsorbed molecules cannot diffuse freely on the surface to arrange a well ordered structure at RT. The activation energy of the surface diffusion is strongly increased by two covalent bonds per molecule to the substrate, so that the system cannot overcome the energy barrier without any energy input. Thereupon the samples prepared at room temperature have been annealed at 70 °C in a vacuum chamber for about 1 h and overnight. Only after that could high-resolution STM images be obtained. UHV IRRAS data were recorded for the MMBT-SAMs prepared at these two different temperatures in order to exclude degradation of the monolayer during annealing (see section on IRRAS). For a detailed discussion of the structural models the high-resolution images of the MMBT-SAMs prepared at 70 °C are used. The micrograph (e) in Fig. 5 reveals the presence of three different rotational domains with a relative orientation of 60° to each other and a length of about 40 nm. A detailed analysis of the structures in the high-resolution STM image (f) exhibits a periodic structure with a $(3 \times \sqrt{3})$ rectangular unit cell. For the samples which have been annealed overnight at 70 °C (in Fig. 5g) bigger domain sizes are observed and the vacancy islands also grow. A height profile analysis of image (g) reveals that all steps visible have the same height, which within experimental error corresponds to the step height of a Au(111) step, *i.e.* 2.4 Å. The origin of the different feature in the morphology in images (c) and (g) can be attributed to the pronounced stress induced by the binding of the bidentate anchors to the substrate. The resulting change in surface morphology is obviously increased by annealing. A closer inspection of the high-resolution data (i) reveals, however, that the molecules adopt the same molecular arrangement as observed for shorter annealing times.

We have compared the experimental STM images with the simulated ones. In Fig. 6(a) a section of the micrograph (f) in Fig. 5 is shown. The electron density of the adsorbed MMBT molecule is distributed obviously perpendicular to the row of molecules. STM-Simulations of MMBT adsorbed in a monolayer with the experimentally determined unit cell $(3 \times \sqrt{3})$ show that the perpendicular orientation of the charge density relative to the row of molecules is realized if both S-atoms occupy equal adsorption sites: both S-atoms adsorb above a bridge position with both S-atoms being slightly shifted either towards an fcc or towards an hcp hollow site. These two possibilities cannot be distinguished in STM images. However, if one S-atom is shifted towards the fcc hollow site and the other one towards the hcp hollow site the electron density is no longer distributed perpendicularly to the row of molecules but rather reveals an angle of about 60°. Other adsorption sites for the sulfur atoms were found to not be stable.

Although the energetic differences between the four stable adsorption sites are rather small (DFT: 0.03 eV, DFT-D: 0.12 eV at most), the adsorption configurations in which both S-atoms

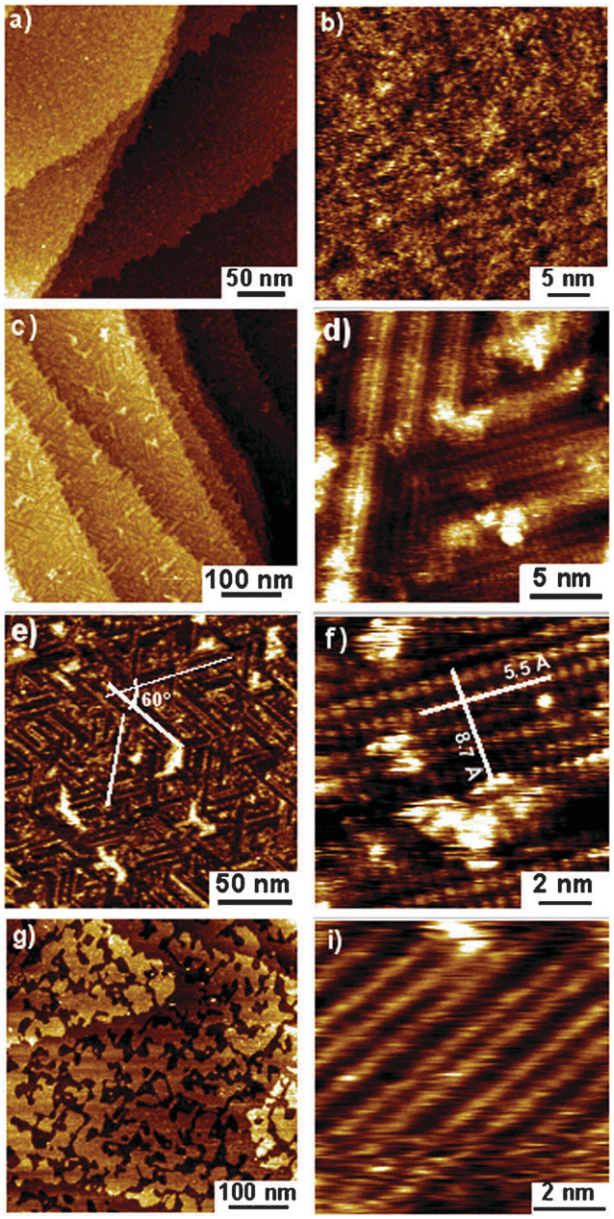

Fig. 5 STM images of MMBT-SAMs (a) and (b) prepared at RT; (c)–(f) annealed for about 1 h at 70 °C; (g) and (i) annealed overnight at 70 °C. With the help of these images a $(3 \times \sqrt{3})$ unit cell can be determined for the MMBT monolayer.

occupy equal adsorption sites, in particular the fcc shifted bridge position, are slightly preferred. For SAMs made from monothiols a similar adsorption site for the S-atoms has been observed.[62,63] However, a number of other works corroborate strongly the on-top positions.[64]

For the positive sample bias used to record these STM-data, unoccupied states of the system are probed. In the lowest unoccupied molecular orbitals both the S-atoms and the ring-C-atoms are involved. Since the C-atoms of the phenyl ring are located much higher than the S-atoms, the delocalized π-electron system of the phenyl ring appears as a bright spot in the constant-current STM images. On closer inspection of the simulated data even the electron density located at the S-atoms

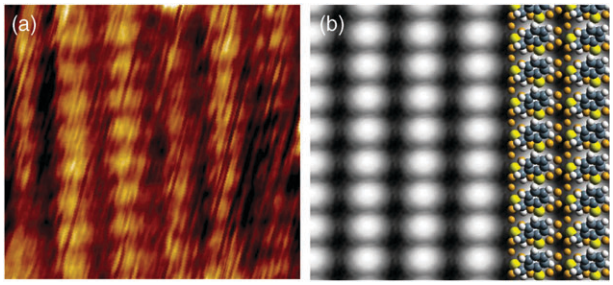

Fig. 6 Comparison of experimental and simulated STM images. (a): experimental STM image of MMBT SAM after 1 h annealing at 70 °C (V_{sample} = +0.9 V, I_t = 60 pA). (b): simulated STM image for a $(3 \times \sqrt{3})$ unit cell (V_{sample} = +0.9 V, isosurface value = 1.8×10^{-5} electrons Å^{-3}). On the right the structure used for the simulation of the STM image is superposed. Both sulfur atoms of the MMBT molecule adsorb on bridge adsorption sites shifted towards an fcc hollow site. This superlattice exhibits the highest adsorption energy of all calculated superlattices showing other adsorption sites for sulfur.

can indeed be seen as weak spots in between the bright spots assigned to the phenyl rings.

TDS data

Fig. 7 displays the averaged TDS data, which is recorded for m/z = 154 amu (*i.e.*, the mass of the molecule ions). The main signature in the spectrum recorded for the molecular mass is a pronounced double peak starting at around 350 K with two maxima located at 393 and 427 K. To determine the binding energy, which is assumed to be equal to the activation energy for desorption, we will only consider the first peak, because the additional peak at higher energy may result from thermally induced reactions within the aromatic SAMs occurring at higher temperatures. Assuming that the pre-exponential factor is the same as that reported for phenylthiol, 9.9×10^{15} s^{-1}, a Redhead-analysis of the temperatures yields a binding energy of 1.35 eV. Desorption of monomeric diradicals is considered to be highly unlikely, because the calculated binding energy of a MMBT diradical onto a Au(111) surface amounts to 3.39 eV, much larger than the experimentally determined value of 1.35 eV. A similar desorption temperature, 427 K, corresponding to a desorption energy of 1.47 eV was reported for SAMs made from benzenethiol on Au(111) substrates by Käfer *et al.*[65] We propose that the thermally induced desorption of benzenethiol proceeds *via* the formation of Ph–S–S–Ph dimers. Such a desorption mechanism involving the formation of S–S disulfide bonds between two adjacent thiolate species is likely to also govern the desorption of the MMBT-based SAMs. In contrast to such an intermolecular S–S bond formation for the MMBT we propose the formation of an intramolecular S–S bond (see Fig. 8). This assumption is corroborated by DFT-D calculations. When taking such a 5-membered disulfide ring system (dithiolane) as a reference the binding energy of MMBT on Au(111) is calculated to be 1.22 eV. Considering the experimental error, the error induced by the pre-exponential factor used to calculate the desorption energies, the errors induced by DFT as well as the estimation of the dispersive interactions, the dispersion-corrected calculated desorption energy compares well with the experimental one of 1.35 eV.

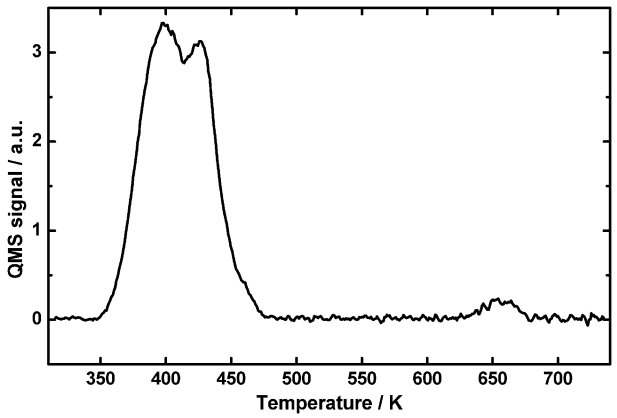

Fig. 7 TDS spectrum of MMBT SAM recorded for $m/z = 154$ amu at a heating rate of $\beta = 0.5$ K s^{-1}.

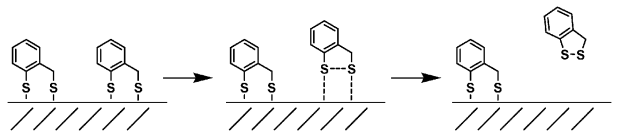

Fig. 8 Proposed desorption mechanism of the MMBT-based SAMs. The molecules desorb by means of the formation of a dithiolane molecule building an intramolecular S–S bond.

Proposed model of the structure of the MMBT-SAM on Au(111)

Our results obtained by a number of complementary techniques and theoretical simulations indicate that the MMBT molecule forms a well-defined SAM on the Au(111) surface. The absence of a number of bands seen for bulk MMBT in the SAM IRRAS data results from the surface selection rule and indicates a preferential orientation of the MMBT molecule relative to the surface. For the first time, molecular resolution was achieved in STM micrographs recorded for SAMs made from a bidentate dithiol. Theoretical calculations employing DFT for a slab with the experimentally determined $(3 \times \sqrt{3})$ unit cell revealed good agreement with the experimentally obtained STM-micrographs and binding energy. Structural models where each MMBT forms only one thiolate-bond to the surface have also been considered. We feel, however, that we can rule out the presence of such species since in the experimental data no indication for the S–H vibration expected for the remaining thiol-species was seen and since the theoretical results suggested that the di-thiolate structure is significantly more stable ($E_{\mathrm{bind}} = 3.39$ eV per molecule).

The structure of the MMBT-SAM on Au(111) as obtained from the theoretical results is shown in Fig. 9. The energetically most favourable structure is one where both S-atoms occupy fcc shifted bridge positions and a phenyl-plane tilt angle of 41.5° relative to the surface normal. The resulting thickness amounts to 6.1 Å. The simulated STM images are in good agreement with the experimental ones (Fig. 6). Additionally, an *ab initio* thermodynamics analysis shows that indeed the $(3 \times \sqrt{3})$ structure is the most stable unit cell with respect to the free adsorption energy over a broad range of the chemical potential (Fig. 10).[66] Furthermore, the experimental

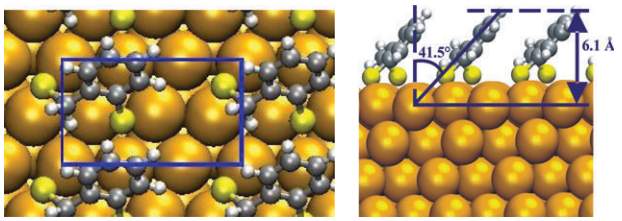

Fig. 9 Proposed structure of the MMBT-SAM on Au(111) as obtained from the DFT-calculations (see text). The MMBT molecule adsorbs with both S-atoms occupying fcc shifted bridge positions and with its phenyl ring tilted by 41.5° away from the surface normal; the thickness of a MMBT monolayer (height of the top H-atom above a plane going through the top layer of Au atoms) amounts to 6.1 Å.

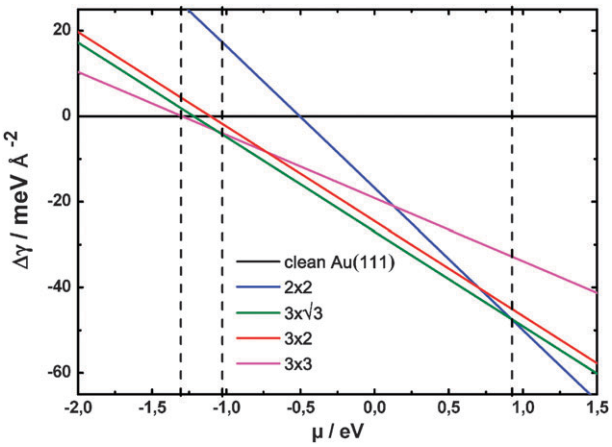

Fig. 10 Free energy of adsorption of MMBT on Au(111) as a function of the chemical potential of MMBT. The $(3 \times \sqrt{3})$ structure is stable over a broad range of the chemical potential.

desorption energy as determined from the first maximum in the TDS-data, 1.35 eV, agrees rather well with the theoretical data when assuming that desorption takes place *via* formation of an intramolecular disulfide bond.

On the basis of the theoretical results we propose that the MMBT molecule adsorbs by forming two Au–S covalent bonds to the Au(111) surface. The preferred adsorption positions for the two S-atoms are the fcc shifted bridge positions. Note that also for SAMs made from monothiols a similar adsorption site is seen for the S-atoms.[62,63]

Conclusions

In conclusion, we find that after annealing SAMs made from an aromatic organodithiol, 2-mercaptomethylbenzenethiol is yielded out of ethanolic solution, on an Au-substrate organic adlayers exhibiting a high degree of lateral order as demonstrated by molecular resolution STM micrographs. Spectroscopic data from XPS and IRRAS are fully consistent with the presence of a well defined monolayer with a $(3 \times \sqrt{3})$ unit cell containing one molecule. Slab calculations using DFT provide very good agreement between theoretical and experimental data by assuming the presence of dithiolate species with both S-atoms adsorbed in near-bridge positions similar to the adsorption sites observed for monothiol based SAMs. Our results indicate that also for organic compounds anchored to

the substrate *via* two thiolate bonds a high degree of structural order can be achieved by annealing the SAM to appropriate temperatures.

Acknowledgements

This work has been partially supported by the European Union (FP6 STReP SURMOF, NMP4-CT-2006-032109). We thank the bwGRiD project for computational resources.[67]

References

1 F. Schreiber, *Prog. Surf. Sci.*, 2000, **65**(5–8), 151–256.
2 J. C. Love, L. A. Estroff, J. K. Kriebel, R. G. Nuzzo and G. M. Whitesides, *Chem. Rev.*, 2005, **105**(4), 1103–1169.
3 A. Ulman, *Self-Assembled Monolayers of Thiols*, Elsevier Science and Technology, Amsterdam, 1998, vol. 24.
4 P. E. Laibinis, G. M. Whitesides, D. L. Allara, Y. T. Tao, A. N. Parikh and R. G. Nuzzo, *J. Am. Chem. Soc.*, 1991, **113**(19), 7152–7167.
5 P. E. Laibinis, R. G. Nuzzo and G. M. Whitesides, *J. Phys. Chem.*, 1992, **96**(12), 5097–5105.
6 K. Edinger, A. Gölzhäuser, K. Demota, C. Wöll and M. Grunze, *Langmuir*, 1993, **9**(1), 4–8.
7 M. Kind and C. Wöll, *Prog. Surf. Sci.*, 2009, **84**(7–8), 230–278.
8 J. Liu, L. Stratmann, S. Krakert, M. Kind, F. Olbrich, A. Terfort and C. Wöll, *J. Electron Spectrosc. Relat. Phenom.*, 2009, **172**(1–3), 120–127.
9 R. Arnold, W. Azzam, A. Terfort and C. Wöll, *Langmuir*, 2002, **18**(10), 3980–3992.
10 T. T. Wooster, P. R. Gamm, W. E. Geiger, A. M. Oliver, A. J. Black, D. C. Craig and M. N. PaddonRow, *Langmuir*, 1996, **12**(26), 6616–6626.
11 S. Lee, Y. S. Shon, R. Colorado, R. L. Guenard, T. R. Lee and S. S. Perry, *Langmuir*, 2000, **16**(5), 2220–2224.
12 J. M. Tour, L. Jones, D. L. Pearson, J. J. S. Lamba, T. P. Burgin, G. M. Whitesides, D. L. Allara, A. N. Parikh and S. V. Atre, *J. Am. Chem. Soc.*, 1995, **117**(37), 9529–9534.
13 H. A. Biebuyck, C. D. Bian and G. M. Whitesides, *Langmuir*, 1994, **10**(6), 1825–1831.
14 R. G. Nuzzo and D. L. Allara, *J. Am. Chem. Soc.*, 1983, **105**(13), 4481–4483.
15 R. G. Nuzzo, F. A. Fusco and D. L. Allara, *J. Am. Chem. Soc.*, 1987, **109**(8), 2358–2368.
16 K. Bandyopadhyay, M. Sastry, V. Paul and K. Vijayamohanan, *Langmuir*, 1997, **13**(4), 866–869.
17 N. Garg, J. M. Friedman and T. R. Lee, *Langmuir*, 2000, **16**(9), 4266–4271.
18 K. Rajalingam, T. Strunskus, A. Terfort, R. A. Fischer and C. Wöll, *Langmuir*, 2008, **24**(15), 7986–7994.
19 A. Niklewski, W. Azzam, T. Strunskus, R. A. Fischer and C. Wöll, *Langmuir*, 2004, **20**(20), 8620–8624.
20 Y. S. Shon, R. Colorado, C. T. Williams, C. D. Bain and T. R. Lee, *Langmuir*, 2000, **16**(2), 541–548.
21 Y. S. Shon, S. Lee, R. Colorado, S. S. Perry and T. R. Lee, *J. Am. Chem. Soc.*, 2000, **122**(31), 7556–7563.
22 S. S. Perry, S. Lee, Y. S. Shon, R. Colorado and T. R. Lee, *Tribol. Lett.*, 2001, **10**(1/2), 81–87.
23 J. S. Park, A. C. Smith and T. R. Lee, *Langmuir*, 2004, **20**(14), 5829–5836.
24 H. Azehara, W. Mizutani, Y. Suzuki, T. Ishida, Y. Nagawa, H. Tokumoto and K. Hiratani, *Langmuir*, 2003, **19**(6), 2115–2123.
25 R. C. Sabapathy, S. Bhattacharyya, M. C. Leavy, W. E. Cleland and C. L. Hussey, *Langmuir*, 1998, **14**(1), 124–136.
26 J. Kunze, J. Leitch, A. L. Schwan, R. J. Faragher, R. Naumann, S. Schiller, W. Knoll, J. R. Dutcher and J. Lipkowski, *Langmuir*, 2006, **22**(12), 5509–5519.
27 Y. S. Shon and T. R. Lee, *Langmuir*, 1999, **15**(4), 1136–1140.
28 Y. S. Shon, S. Lee, S. S. Perry and T. R. Lee, *J. Am. Chem. Soc.*, 2000, **122**(7), 1278–1281.
29 K. Bandyopadhyay, V. Patil, M. Sastry and K. Vijayamohanan, *Langmuir*, 1998, **14**(14), 3808–3814.
30 K. Bandyopadhyay, K. Vijayamohanan, G. S. Shekhawat and R. P. Gupta, *J. Electroanal. Chem.*, 1998, **447**(1–2), 11–16.
31 N. Garg and T. R. Lee, *Langmuir*, 1998, **14**(14), 3815–3819.
32 K. Bandyopadhyay, K. Vijayamohanan, M. Venkataramanan and T. Pradeep, *Langmuir*, 1999, **15**(16), 5314–5322.
33 K. Murty, M. Venkataramanan and T. Pradeep, *Langmuir*, 1998, **14**(19), 5446–5456.
34 S. W. Joo, S. W. Han and K. Kim, *J. Phys. Chem. B*, 1999, **103**(49), 10831–10837.
35 S. W. Joo, S. W. Han and K. Kim, *J. Colloid Interface Sci.*, 2001, **240**(2), 391–399.
36 N. Garg, E. Carrasquillo-Molina and T. R. Lee, *Langmuir*, 2002, **18**(7), 2717–2726.
37 J. K. Lim, Y. Kim, O. Kwon and S. W. Joo, *ChemPhysChem*, 2008, **9**(12), 1781–1787.
38 A. G. Hortmann, A. J. Aron and A. K. Bhattacharya, *J. Org. Chem.*, 1978, **43**(17), 3375–3378.
39 E. Klingsberg and A. M. Schreiber, *J. Am. Chem. Soc.*, 1962, **84**(15), 2941–2944.
40 H. Noei, H. S. Qiu, Y. M. Wang, E. Löffler, C. Wöll and M. Muhler, *Phys. Chem. Chem. Phys.*, 2008, **10**(47), 7092–7097.
41 C. Rohmann, Y. M. Wang, M. Muhler, J. Metson, H. Idriss and C. Wöll, *Chem. Phys. Lett.*, 2008, **460**(1–3), 10–12.
42 Y. M. Wang and C. Wőll, *Surf. Sci.*, 2009, **603**(10–12), 1589–1599.
43 O. Shekhah, N. Roques, V. Mugnaini, C. Munuera, C. Ocal, J. Veciana and C. Wöll, *Langmuir*, 2008, **24**(13), 6640–6648.
44 C. D. Bain, E. B. Troughton, Y. T. Tao, J. Evall, G. M. Whitesides and R. G. Nuzzo, *J. Am. Chem. Soc.*, 1989, **111**(1), 321–335.
45 L. Hallmann, A. Bashir, T. Strunskus, R. Adelung, V. Stämmler, C. Wöll and F. Tuczek, *Langmuir*, 2008, **24**(11), 5726–5733.
46 G. Loepp, S. Vollmer, G. Witte and C. Wöll, *Langmuir*, 1999, **15**(11), 3767–3772.
47 P. Feulner and D. Menzel, *J. Vac. Sci. Technol.*, 1980, **17**(2), 662–663.
48 G. Kresse and J. Furthmuller, *Phys. Rev. B: Condens. Matter*, 1996, **54**(16), 11169–11186.
49 G. Kresse and J. Furthmuller, *Comput. Mater. Sci.*, 1996, **6**(1), 15–50.
50 J. P. Perdew, K. Burke and M. Ernzerhof, *Phys. Rev. Lett.*, 1996, **77**(18), 3865–3868.
51 P. E. Blochl, *Phys. Rev. B: Condens. Matter*, 1994, **50**(24), 17953–17979.
52 G. Kresse and D. Joubert, *Phys. Rev. B: Condens. Matter Mater. Phys.*, 1999, **59**(3), 1758–1775.
53 S. Grimme, *J. Comput. Chem.*, 2004, **25**(12), 1463–1473.
54 S. Grimme, *J. Comput. Chem.*, 2006, **27**(15), 1787–1799.
55 M. J. Frisch, G. W. Trucks, H. B. Schlegel, G. E. Scuseria, M. A. Robb, J. R. Cheeseman, J. A. J. Montgomery, T. Vreven, K. N. Kudin, J. C. Burant, J. M. Millam, S. S. Iyengar, J. Tomasi, V. Barone, B. Mennucci, M. Cossi, G. Scalmani, N. Rega, G. A. Petersson, H. Nakatsuji, M. Hada, M. Ehara, K. Toyota, R. Fukuda, J. Hasegawa, M. Ishida, T. Nakajima, Y. Honda, O. Kitao, H. Nakai, M. Klene, X. Li, J. E. Knox, H. P. Hratchian, J. B. Cross, V. Bakken, C. Adamo, J. Jaramillo, R. Gomperts, R. E. Stratmann, O. Yazyev, A. J. Austin, R. Cammi, C. Pomelli, J. W. Ochterski, P. Y. Ayala, K. Morokuma, G. A. Voth, P. Salvador, J. J. Dannenberg, V. G. Zakrzewski, S. Dapprich, A. D. Daniels, M. C. Strain, O. Farkas, D. K. Malick, A. D. Rabuck, K. Raghavachari, J. B. Foresman, J. V. Ortiz, Q. Cui, A. G. Baboul, S. Clifford, J. Cioslowski, B. B. Stefanov, G. Liu, A. Liashenko, P. Piskorz, I. Komaromi, R. L. Martin, D. J. Fox, T. Keith, M. A. Al-Laham, C. Y. Peng, A. Nanayakkara, M. Challacombe, P. M. W. Gill, B. Johnson, W. Chen, M. W. Wong, C. Gonzalez and J. A. Pople, Gaussian, Inc., Wallingford, CT, 2004.
56 J. Tersoff and D. R. Hamann, *Phys. Rev. B: Condens. Matter*, 1985, **31**(2), 805.
57 C. Fuxen, W. Azzam, R. Arnold, G. Witte, A. Terfort and C. Wöll, *Langmuir*, 2001, **17**(12), 3689–3695.
58 M. Born and E. Wolf, *Principles of Optics*, Cambridge University Press, Cambridge, 2nd edn, 1999.
59 G. Heimel, L. Romaner, J. L. Bredas and E. Zojer, *Surf. Sci.*, 2006, **600**(19), 4548–4562.

60 G. Heimel, L. Romaner, J. L. Bredas and E. Zojer, *Langmuir*, 2008, **24**(2), 474–482.
61 A. Turchanin, D. Käfer, M. El-Desawy, C. Wöll, G. Witte and A. Gölzhäuser, *Langmuir*, 2009, **25**(13), 7342–7352.
62 J. Kucera and A. Gross, *Langmuir*, 2008, **24**(24), 13985–13992.
63 Y. Yourdshahyan and A. M. Rappe, *J. Chem. Phys.*, 2002, **117**(2), 825–833.
64 J. A. Rodriguez, J. Dvorak, T. Jirsak, G. Liu, J. Hrbek, Y. Aray and C. Gonzalez, *J. Am. Chem. Soc.*, 2003, **125**(1), 276–285.
65 D. Käfer, A. Bashir and G. Witte, *J. Phys. Chem. C*, 2007, **111**(28), 10546–10551.
66 K. Reuter and M. Scheffler, *Phys. Rev. B: Condens. Matter Mater. Phys.*, 2001, **65**(3), 035406.
67 bwGRiD, member of the German D-Grid initiative, funded by the Ministry for Education and Research (Bundesministerium für Bildung und Forschung) and the Ministry for Science, Research and Arts Baden-Wuerttemberg (Ministerium für Wissenschaft, Forschung und Kunst Baden-Wuerttemberg) http://www.bw-grid.de.